Porphyrin Protonation Studied by Magnetic Circular Dichroism

ARTICLE *in* THE JOURNAL OF PHYSICAL CHEMISTRY A · DECEMBER 2011

Impact Factor: 2.69 · DOI: 10.1021/jp2105192 · Source: PubMed

4 AUTHORS, INCLUDING:

Valery Andrushchenko
Academy of Sciences of the Czech Republic
56 PUBLICATIONS **899** CITATIONS
SEE PROFILE

Kenneth Ruud
University of Tromsoe
343 PUBLICATIONS **8,654** CITATIONS
SEE PROFILE

THE JOURNAL OF PHYSICAL CHEMISTRY A

ARTICLE

pubs.acs.org/JPCA

Porphyrin Protonation Studied by Magnetic Circular Dichroism

Petr Štěpánek,*[,†,‡] Valery Andrushchenko,[†] Kenneth Ruud,[§] and Petr Bouř*[,†]

[†]Institute of Organic Chemistry and Biochemistry, Academy of Sciences, Flemingovo nám. 2, 16610 Prague, Czech Republic

[‡]Faculty of Mathematics and Physics, Charles University, Ke Karlovu 5, Prague, 121 16 Czech Republic

[§]Centre for Theoretical and Computational Chemistry, Department of Chemistry, University of Tromsø, N-9037 Tromsø, Norway

ABSTRACT: Magnetic circular dichroism (MCD) spectroscopy provides valuable information about electronic excited states in molecules. The interpretation of spectra is however difficult, often requiring additional theoretical calculations to rationalize the observed signal. Recent developments in time-dependent density functional theory (TDDFT) bring hope that the applicability of MCD spectroscopy for chemical problems may be significantly extended. In this study, two modern analytical TDDFT implementations are compared and used to understand experimental MCD spectra of a model porphyrin system upon protonation. Changes in porphyrin geometry and electronic structure are related to MCD intensities by comparing the spectra of 5,10,15,20-tetraphenyl-21*H*,23*H*-porphyrintetrasulfonic acid (TPPS) measured at different pH values with the TDDFT calculations. Although the theoretical results slightly depended on the chosen exchange−correlation functional, the computations provided MCD curves that could well rationalize the experimental data. The protonation of the porphyrin core causes marked changes in the MCD spectrum, whereas the role of the substituents is limited. Also, different conformations of the porphyrin substituents cause relatively minor changes of the MCD pattern, mostly in the Soret region, where the porphine and phenyl electronic transitions start to mix. The solvent environment simulated by the dielectric model caused a shift (∼20 nm) of the absorption bands but only minor variations in the absorption and MCD spectral shapes. The study thus demonstrates that the recently available first-principles interpretations of MCD spectra significantly enhance the applicability of the technique for molecular structural studies.

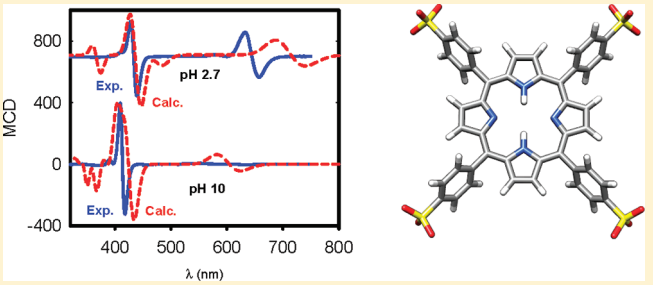

INTRODUCTION

Magnetic circular dichroism (MCD) is a well-established spectroscopic technique that measures the differential absorption of left and right circularly polarized light in the ultraviolet, visible, or NIR region.[1] The chirality of the sample is induced by a static magnetic field oriented along the light beam. Modern computations of MCD spectra are largely based on the theoretical analysis of Stephens,[2,3] who analyzed the perturbed molecular wave function in order to derive expressions for the different interaction mechanisms that contribute to observed MCD intensities. Because of the complicated mathematics and limited computational tools, however, semiempirical interpretation approaches have been preferred for a long time.[4,5] There have been early implementations of the MCD "B term" at the Hartree−Fock and multiconfigurational self-consistent field levels of theory by Jensen and co-workers[6,7] and Coriani et al.,[8] as well as implementations at the coupled-cluster level.[8,9] A quasi-relativistic formulation was applied to the CH_3I molecule[10] and other test systems.[11] However, it is only recently that MCD simulations within the time-dependent DFT (TDDFT) framework have been made available[12−14] in a few program packages,[15,16] allowing for calculations on larger molecules.

Although the chemical and analytical applications of MCD coupled with first-principles interpretations are still relatively rare, previous work has already demonstrated the potential of the technique. For example, MCD helped to decipher the electronic structure of vitamin B_{12}.[17] Quite often, inorganic[18] and organic[19,20] metal complexes are studied.

In this work, we investigate how the combined theoretical and experimental MCD spectra can be used for studying a typical chemical reaction, the porphyrin protonation. The changes in the electronic structure are reflected in the MCD spectrum. As a model compound, the 5,10,15,20-tetraphenyl-21*H*,23*H*-porphyrintetrasulfonic acid anion $TPPS^{4-}$ and its protonated form H_2TPPS^{2-} were chosen as they are relatively small, rigid, and very soluble in water (see Scheme 1).

The TPPS protonation mechanism and proton transfer in porhyrins have attracted attention in several studies[21] because of the abundance of the porphyrin backbone in living organisms and biomolecular structures.[22] The porphyrin acid−base equilibria are, in particular, important for physicochemical properties, such as passive diffusion through the plasmic membrane.[23] TPPS itself was proposed as a singlet oxygen generator and is thus suitable as a drug for photodynamic treatment of certain cancerous tumors.[24]

Received: November 2, 2011
Revised: December 2, 2011
Published: December 05, 2011

Scheme 1. Structure of $TPPS^{4-}$ and H_2TPPS^{2-}

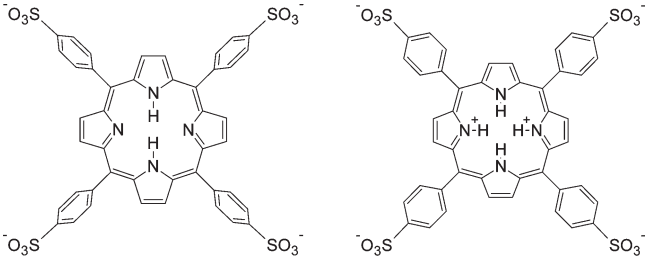

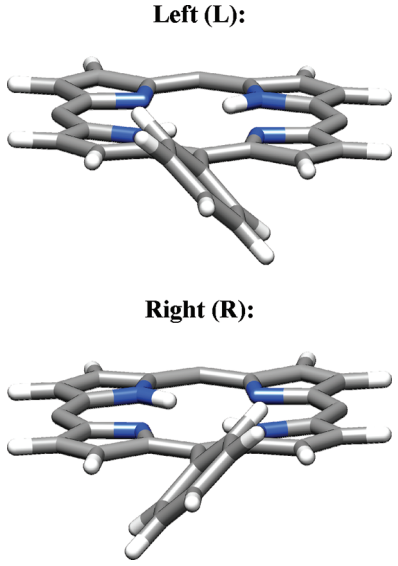

Figure 1. Definition of the phenyl dihedral angles.

Acidobasic properties of porphyrins can be important for this process. For example, the interstitial pH in malignant cells (about 7.0) is lower than that in normal tissues (mean pH of 7.5).[25]

On the basis of titration experiments, the inner core porphyrin nitrogen atoms were identified as the proton binding sites, producing distinct changes in the absorption spectra.[26] As discussed below, this is also consistent with our experimental and theoretical MCD results. However, the environment had to be included in the computation to balance the hydrogen charge. The polarizable continuum model (PCM) approach was chosen to account for the solvent as it has been shown to give a fairly balanced description of the MCD intensities of solvated molecules at a reasonable computational cost.[27]

As the computations including the environment are quite demanding, a simpler tetraphenylporphyrin subsystem was chosen for some MCD computations performed at a higher level of theory. The role of substituents was estimated from trial computations of MCD or absorption spectra. They influence the spectra only in a minor way, in agreement with the observations made in a CD spectral study.[28] Finally, we explore the importance of molecular flexibility, which could be included at least partially by a computation of the phenyl group rotamers. Interestingly, some parts of MCD spectrum were found to be quite sensitive to the conformational structure.

METHOD

Experimental Section. Commercial TPPS (disodium salt, Sigma-Aldrich) was dissolved in MilliPore water (pH ≈ 6). The pH was adjusted by 0.1 M HCl and 0.1 M NaOH to 2.7 and 10.0; the TPPS concentration was 4 μM (40 μM for pH 10.0 and the Q-band region). MCD and absorption spectra were measured at room temperature with the Jasco J-815 spectrometer equipped with 1.5 T permanent magnet. The samples were contained in a rectangular fused silica cell of 1 cm optical path length, and the spectra were recorded within 300−750 nm at 1 nm resolution, a response time of 16 s, and a scanning speed of 5 nm/min. Spectra of two accumulations were averaged.

Calculations. The Turbomole program[29] was employed for geometry optimization. Calculations were performed with the BP86[30] functional and def-TZVPP[31] basis set using the resolution of identity (RI) approximation. The COSMO solvent model[32] was used to describe the aqueous environment.

All $TPPS^{4-}$ conformers differing by the phenyl group rotation (Figure 1) were generated, which provided $2^4 = 16$ structures. Using the same notation as that introduced previously for tetraphenylporphyrin,[33] the conformers of unprotonated $TPPS^{4-}$ were divided into five classes differing in symmetry, LRRL (C_{2h}), LRLR (C_{2v}), LLRR (C_{2h}), LRLL (C_1), and LLLL (D_2). The latter two groups also generate enantiomers, that is, LLLL in our convention also comprises RRRR and so forth.

The Gaussian software[34] was used for calculation of the electronic absorption spectra. The exchange−correlation (XC) functionals tested for the TPPS system were B3LYP,[35] BP86,[30] BPW91,[36] BLYP,[35] and CAM-B3LYP[37] functionals. The influence of the basis set size on the absorption properties of the porphyrin chromophore was tested on tetraphenylporphyrin (TPP) with the 6-31G, 6-31G*, 6-31+G, 6-31+G*, 6-311++G**, and cc-pVTZ basis sets. The COSMO variant of the PCM solvent model was used with the united atom topological model for the cavity (UA0).[34]

For theoretical MCD intensities, we used the SAOP functional[38] as implemented in the ADF[16] program with the TZP basis set. In addition, the intensities were also computed by Dalton[15] using the B3LYP/6-31+G* and B3LYP/6-31G approximation levels and the IEF-PCM solvent model.[39] Although it is often advocated to use the Coulomb-attenuated B3LYP (CAM-B3LYP) functional for studies of excited states,[40] in this work, we will focus entirely on valence-excited states, for which B3LYP generally performs better.[41]

Absorption spectra calculated with the Gaussian program and the ADF MCD intensities were convoluted with a Gaussian curve to mimic the experimental spectrum, with the full width at half height corresponding to 0.1 eV (~20−30 nm). The Dalton computation provides the spectral curves directly; the spectral width was controlled by a damping factor of 0.1 eV, and excitation energies were selected to provide 10 nm equidistant spacing within the spectral range 300−700 nm.

RESULTS AND DISCUSSION

Geometry. As previously reported for TPP,[33] the phenyl rotation barrier is quite low, and the differences in relative conformer energies are small. Therefore, the Boltzmann equilibrium of more conformers can be expected also for TPPS. Calculated $TPPS^{4-}$ relative conformer energies and populations at 300 K are summarized in Table 1. The lowest-energy $TPPS^{4-}$

Table 1. Calculated Relative Energies (E, kJ/mol) and Boltzmann Populations (η, %, at 300 K) of $TPPS^{4-}$ Conformers

conformer symmetry	degeneracy	E^a	E^b	E^c	$E_{TPP}{}^d$	η^a
LRLR C_{2v}	2	0	0	0	0	44
LLRR C_{2h}	2	2.5	1.6	2.9	4.8	17
LRRL C_{2h}	2	2.8	0.4	2.7	5.2	13
LLLL D_2	2	3.7	1.9	4.8	2.4	10
LRLL C_1	8	5.9	4.4	2.4	1.2	16

[a] BP86/def-TZVPP/COSMO. [b] B3LYP/def-TZVPP/COSMO single-point energies for BP86/def-TZVPP/COSMO geometries. [c] BPW91/6-31G*. [d] For TPP, BPW91/6-31G*; ref 33.

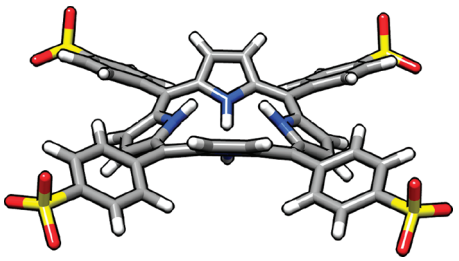

Figure 2. Optimized (BP86/def-TZVPP/COSMO) geometry of H_2TPPS^{2-}.

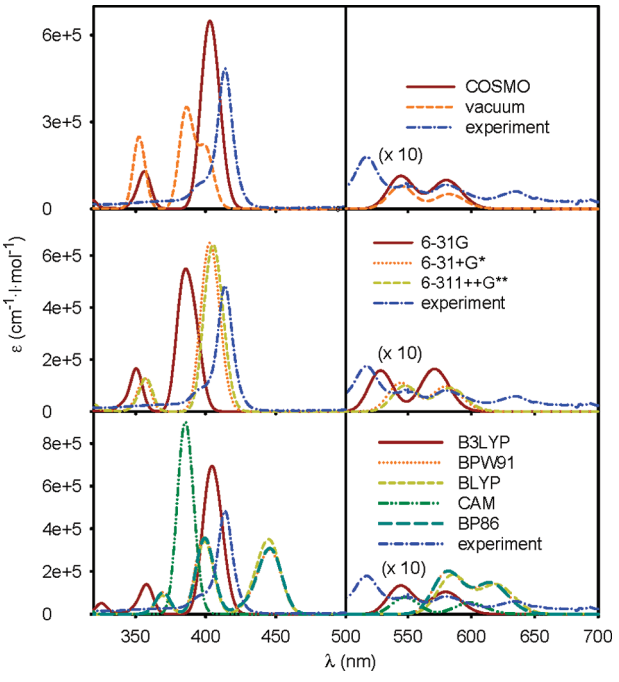

Figure 3. Calculated TPP absorption by several theoretical models (variations of the default B3LYP/6-31+G*/COSMO combination are indicated) and the experimental TPPS spectra.

conformer is LRLR, as for TPP.[42] Note that the conformer populations are also significantly influenced by the entropic degeneracy factor. In particular, the eight-times degenerate LRLL conformer is more frequent than a lower-energy one, LLLL.

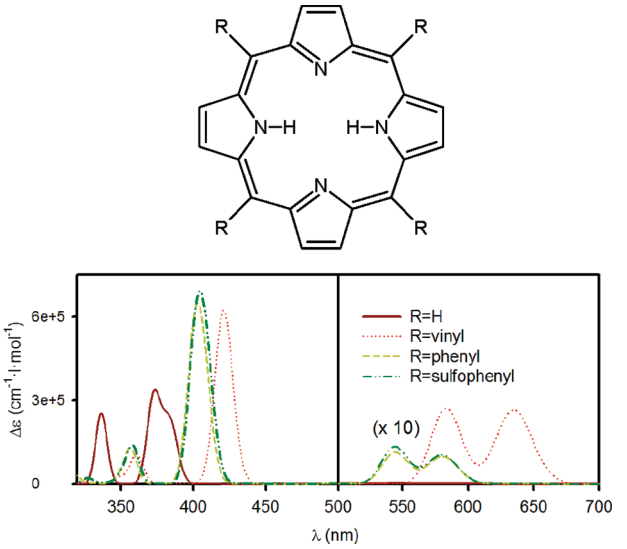

Figure 4. Substituent influence: Calculated B3LYP/6-31+G*/COSMO absorption spectra of porphyrine, tetravinylporphine, and tetraphenyl- and tetra(sulfophenyl)-porphine.

The flexibility of $TPPS^{4-}$ contrasts with that of H_2TPPS^{2-}, where all of the LRLR, LLRR, LRRL, LLLL, and LRLL starting structures converged to the same C_{2v} conformer. This is caused by the distortion of the porphine core induced by the protonation, which enforces the conformation of the attached phenyl rings (Figure 2).

Geometries of $TPPS^{4-}$ and H_2TPPS^{2-} optimized with and without the COSMO aqueous correction were quite similar, as can be expected because the conformation is primarily controlled by the nonpolar phenyl and porphyrin groups.

Functional, Basis Set, and Solvent Effects. The dependence of the electronic transition energies and absorption intensities on the choice of the XC functional (B3LYP, BP86, BPW91, BLYP, and CAM-B3LYP), basis set (6-31G, 6-31+G*, and 6-311++G**), and environment for the TPP test system can be seen in Figure 3. The COSMO aqueous correction improves the position of the Soret band (top part of Figure 3). The vacuum computation provides a maximum at 385 nm, which shifts to 404 nm, closer to the experimental value (for TPPS) of 413 nm. Surprisingly, the "Q" bands at ~570 nm are almost unaffected by the solvent; in porphyrin experiments, they are somewhat hidden in the background or overlapped by vibrational satellites.[43,44] Thus, the two maxima at 544/580 nm calculated with the COSMO solvent most probably correspond to the 551/581 nm experimental signals.

The calculated dependence of the absorption spectrum on the basis set size (middle part of Figure 3) is relatively modest, in agreement with other studies on porphyrins.[45] The smallest 6-31G basis set provides wavelengths lower by ~20 nm than the larger ones; 6-31+G* and 6-311++G** basis sets give virtually the same spectrum. The cc-pVTZ results (not shown) also do not significantly differ from 6-31+G*.

The calculated results depend more strongly on the choice of the functional (Figure 3, bottom); B3LYP provides transition frequencies closest to experiment, whereas CAM-B3LYP gives a too low wavelength for the Soret band; the GGA (BPW91 and BLYP) functionals provide too high Soret wavelengths, and they also overestimate the Q-band intensities.

Substituent Influence. Because the MCD computations are time-demanding, we tried to find a simplified model of TPPS that

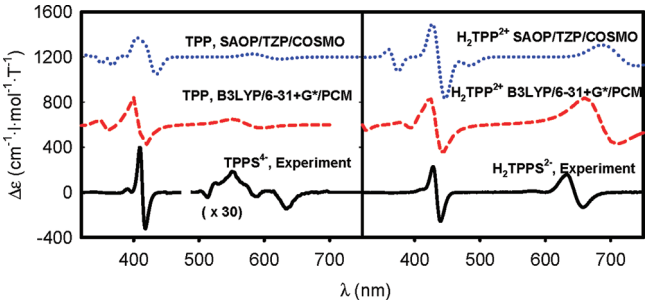

Figure 5. MCD spectra of $TPPS^{4-}$ and H_2TPPS^{2-}: experiment (bottom, solid line, measured at pH = 10 and 2.7 for $TPPS^{4-}$ and H_2TPPS^{2-}, respectively; note the 30× intensity zoom at the higher-wavelength part of the $TPPS^{4-}$ spectrum) and the B3LYP/6-31+G*/PCM (center, dashed line) and SAOP/TZP/COSMO (top, dotted line) simulations.

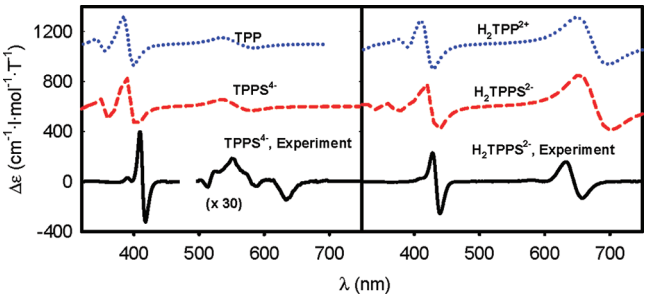

Figure 6. Comparison of calculated B3LYP/6-31G MCD spectra of TPP/H_2TPP^{2+} (top, dotted line) and $TPPS^{4-}/H_2TPPS^{2-}$ (middle, dashed line) with experiment (bottom, solid line, measured at pH = 10.0 and 2.7 for $TPPS^{4-}$ and H_2TPPS^{2-}, respectively).

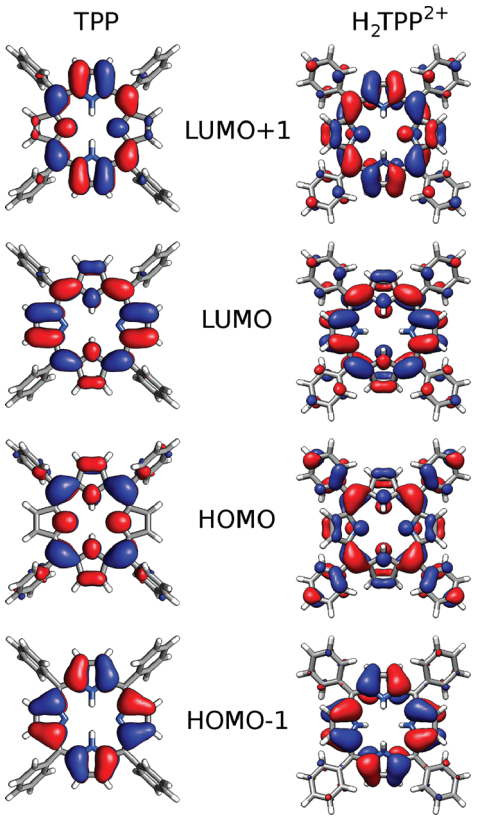

Figure 7. Selected TPP and H_2TPP^{2+} B3LYP/6-31+G*/COSMO orbitals.

could be calculated accurately. We therefore investigated the influence of the distant groups on the porphyrin core absorption properties. Although the porphyrin core π-electron system is known to be relatively isolated,[43,46] it can be significantly perturbed by a substituent. This can also be seen in Figure 4, where the absorption spectra generated for unsubstituted porphine and the vinyl, phenyl, and sulphophenyl derivatives are shown. The plain porphine spectra exhibit a negligible intensity of the Q bands, and the Soret maximum is around 370 nm, clearly split into two components. The vinyl substituent reduces the splitting and causes a significant increase of the Q-band signal. Finally, the phenyl and sulphophenyl residues provide almost the same absorption pattern. In comparison to the vinyl, both the Q and Soret bands are shifted significantly to shorter wavelengths for the phenyl derivative, closer to experiment. The intensity also differs for phenyl and vinyl. We thus conclude that the phenyl analogue can be used as a smaller model system that faithfully simulates the spectrum of TPPS. This leads to a significant reduction of computer time; still, about 5 days were needed for the calculation of the absorption spectrum (2 GHz Intel 64 CPU).

MCD Spectra. In Figure 5, the SAOP/TZP/COSMO (ADF) and B3LYP/6-31+G*/IEF-PCM (Dalton) MCD TPPS spectra are plotted. As in Figure 3 for the absorption spectrum, the GGA functional represented here by SAOP provides transition wavelengths higher than those of the hybrid B3LYP functional. The advantage of the B3LYP approach is apparent primarily for the Q band, where the SAOP central wavelength is 60 nm higher than that in experiment. Interestingly, the SAOP computation provided a much larger number of transitions in the Soret region than B3LYP, as also noted previously.[13] Nevertheless, the resulting band shapes are similar, and both approaches provide reasonable transition energies and realistic spectral patterns, that is, the MCD band signs, if compared to experiment (Figure 5). Interestingly, both methods also provided rather overestimated intensities for the Q-band MCD signals.

In principle, the MCD spectrum can be influenced by the electronic structure of the molecule to a different extent than the absorption spectra. Therefore, we tested the ability of our simplified TPP model to mimic the complete TPPS molecule by calculating the MCD spectra for the latter at a lower computational level. The results are shown in Figure 6, comparing experimental spectra with those calculated for the TPP and TPPS molecules using the B3LYP/6-31G/PCM method. Clearly, the MCD spectra as well as the protonation changes are quite similar for the two molecules. This gives at least some support for the notion that the TPP B3LYP/6-31+G*/PCM computations reflect the results that would be obtained at this computational level also for the TPPS system.

The effect of protonation itself is nicely reproduced by the calculations (Figures 5 and 6). Protonation at the lower pH (right-hand side of the figures) causes an upshift of the Soret (~by 20 nm) and Q-band signals and a significant increase of the intensity of the Q-band MCD signal.

The protonation causes large geometry changes (cf. Figure 2). Rather surprisingly, its effect on the molecular orbitals is limited. Without a full quantum mechanical computation, we would not be able to deduce any relation between the MCD changes and the orbital shapes. For example, the HOMO−1, ..., LUMO+1

dx.doi.org/10.1021/jp2105192 |J. Phys. Chem. A 2012, 116, 778–783

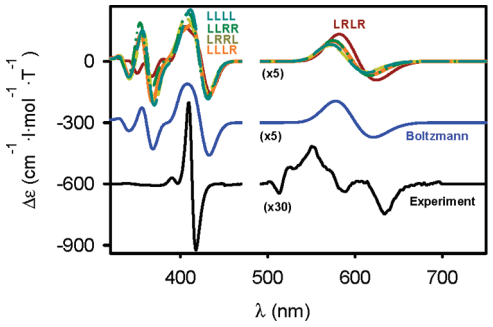

Figure 8. MCD spectra of individual TPP conformers (top), the Boltzmann average (middle), and $TPPS^{4-}$ (bottom) experiment. Spectra were calculated using ADF (SAOP/TZP/COSMO).

TPP and H_2TPP^{2+} orbitals are still very similar (Figure 7). The protonation in H_2TPP^{2+} induces a large involvement of the phenyl rings in the transitions, and a π-conjugation between the phenyl and porphine electrons is enhanced by the deformation of the molecule.

The influence of conformer equilibria and molecular flexibility (modeled by the rotation of the phenyl residues) on the MCD spectrum displayed in Figure 8 is also interesting. Clearly, the main MCD signal (the Soret band) is relatively independent of the conformation. Surprisingly, the most conformer sensitive part is the shortest-wavelength region (below 400 nm). For these transitions, the HOMO/LUMO orbitals do not participate much, whereas the phenyl electrons start to participate. As expected, the lowest-energy conformer MCD spectrum or the Boltzmann average shows the best agreement with experiment, although the computation still overestimates the MCD intensity below 400 nm. To the best of our knowledge, the conformational dependence of MCD was not explored so far. We plan a separate study in the future dedicated to this aspect.

CONCLUSIONS

We have shown that the protonation of TPPS leads to a significant change of the MCD spectral pattern, reproducible by quantum chemical computations. The SAOP functional with the TZP basis set as implemented in ADF provides similar theoretical MCD curves as the B3LYP/6-31+G*/PCM method in Dalton, and both were in agreement with experiment. The energy pattern of the calculated electronic excited states significantly differs for the SAOP and B3LYP functionals, but they provide similar spectra, and comparison with experiment does not allow us to discriminate between these different descriptions. The MCD spectral profile was found to be more sensitive to computational parameters, including the solvent model, basis set, DFT functional, and porphyrin substituents, than absorption. The side-chain rotation did not significantly disturb the basic MCD patterns in the Soret and Q-band regions; however, it did influence the finer spectral features.

The results convincingly show that MCD spectroscopy coupled with ab initio computations can be applied to molecular structural studies. For the porphyrin protonation, it provides additional information about the electronic structure and geometry in comparison to the absorption spectroscopy.

AUTHOR INFORMATION

Corresponding Author

*E-mail: stepanekp@uochb.cas.cz (P.S.); bour@uochb.cas.cz (P.B.).

ACKNOWLEDGMENT

This work was supported by the Czech Science Foundation (P208/11/0105, 203/09/2037, P208/10/0559), Academy of Sciences, Ministry of Education (LH11033), Research Council of Norway (Centre of Excellence Grant 179568/V30), and EU Reintegration Grant (230955).

REFERENCES

(1) Mason, W. R. *A practical guide to magnetic circular dichroism spectroscopy*; Wiley-Interscience: Portland, OR, 2007.
(2) Stephens, P. J. *J. Chem. Phys.* **1970**, *52*, 3489–3516.
(3) Stephens, P. J. *Annu. Rev. Phys. Chem.* **1974**, *25*, 201–232.
(4) Michl, J. *J. Am. Chem. Soc.* **1978**, *100*, 6801–6811.
(5) Michl, J. *J. Am. Chem. Soc.* **1978**, *100*, 6812–6818.
(6) Jensen, J. O.; Adams, G. F.; Chabalowski, C. F. *Chem. Phys. Lett.* **1990**, *172*, 379–387.
(7) Jensen, J. O.; Adams, G. F.; Chabalowski, C. F. *J. Chem. Phys.* **1991**, *94*, 1333–1345.
(8) Coriani, S.; Jorgensen, P.; Rizzo, A.; Ruud, K.; Olsen, J. *Chem. Phys. Lett.* **1999**, *300*, 61–68.
(9) Kjaergaard, T.; Jansik, B.; Jorgensen, P.; Coriani, S.; Michl, J. *J. Phys. Chem. A* **2007**, *111*, 11278–11286.
(10) Honda, Y.; Hada, M.; Ehara, M.; Nakatsuji, H.; Downing, J.; Michl, J. *Chem. Phys. Lett.* **2002**, *355*, 219–225.
(11) Honda, Y.; Hada, M.; Ehara, M.; Nakatsuji, H.; Michl, J. *J. Chem. Phys.* **2005**, *123*, 164113.
(12) Seth, M.; Autschbach, J.; Ziegler, T. *J. Chem. Theory Comput.* **2007**, *3*, 434–447.
(13) Solheim, H.; Ruud, K.; Coriani, S.; Norman, P. *J. Phys. Chem. A* **2008**, *112*, 9615–9618.
(14) Seth, M.; Ziegler, T. Calculation of Magnetic Circular Dichroism Spectra with Time-Dependent Density Functional Theory. In *Advances in Inorganic Chemistry: Theoretical and Computational Inorganic Chemistry*; van Eldik, R., Harvey, J., Eds.; Elsevier: San Diego, CA, 2010; Vol. 62; pp 41−109.
(15) *Dalton, an ab initio electronic structure program*, release 2.0. http://www.daltonprogram.org (2005).
(16) *ADF 2010*; SCM; Theoretical Chemistry, Vrije Universiteit: Amsterdam, The Netherlands, 2007; http://www.scm.com.
(17) Solheim, H.; Kornobis, K.; Ruud, K.; Kozlowski, P. M. *J. Phys. Chem. B* **2011**, *115*, 737–748.
(18) Seth, M.; Ziegler, T.; Autschbach, J. *J. Chem. Phys.* **2005**, *122*, 094112.
(19) Marin, E. H.; Seth, M.; Ziegler, T. *Inorg. Chem.* **2010**, *49*, 6066–6076.
(20) Peralta, G. A.; Seth, M.; Zhekova, H.; Ziegler, T. *Inorg. Chem.* **2008**, *47*, 4185–4198.
(21) Horníček, J.; Dvořáková, H.; Bouř, P. *J. Phys. Chem. A* **2010**, *114*, 3649–3654.
(22) Karlson, P.; Gerok, W.; Gross, W. *Pathobiochemie*; Georg Thieme Verlag: Stuttgart, Germany, 1982.
(23) Brault, D. *J. Photochem. Photobiol., B* **1990**, *6*, 79–86.
(24) Engst, P.; Kubat, P.; Jirsa, M. *J. Photochem. Photobiol., A* **1994**, *78*, 215–219.
(25) Wike-Hooley, J. L.; Haveman, J.; Reinhold, J. S. *Radiother. Oncol.* **1984**, *2*, 343–366.
(26) Farjtabar, A.; Charib, F. *J. Solution Chem.* **2010**, *39*, 231–244.
(27) Solheim, H.; Frediani, L.; Ruud, K.; Coriani, S. *Theor. Chem. Acc.* **2008**, *119*, 231–244.
(28) Šebek, J.; Bouř, P. *J. Phys. Chem. A* **2008**, *112*, 2920–2929.
(29) Ahlrichs, R.; Bar, M.; Baron, H.-P.; Bauernschmitt, R.; Bocker, S.; Ehrig, M.; Eichkorn, K.; Elliot, S.; Furche, F.; Haase, F.; et al. *Turbomole*, version 6; Quantum Chemistry Group, University of Karlsruhe: Karlsruhe, Germany, 1998.
(30) Perdew, J. P. *Phys. Rev. B* **1986**, *33*, 8822–8824.
(31) Schafer, A.; Huber, C.; Ahlrichs, R. *J. Chem. Phys.* **1994**, *100*, 5829–5835.

(32) Klamt, A.; Jonas, V.; Burger, T.; Lohrentz, J. C. W. J. *Phys. Chem. A* **1998**, *102*, 5074–5085.
(33) Bouř, P.; Záruba, K.; Urbanová, M.; Setnička, V.; Matějka, P.; Fiedler, Z.; Král, V.; Volka, K. *Chirality* **2000**, *12*, 191–198.
(34) Frisch, M. J.; Trucks, G. W.; Schlegel, H. B.; Scuseria, G. E.; Robb, M. A.; Cheeseman, J. R.; Scalmani, G.; Barone, V.; Mennucci, B.; Petersson, G. A.; et al. *Gaussian 09*, revision A.02; Gaussian, Inc.: Wallingford CT, 2009; http://www.gaussian.com.
(35) Becke, A. D. *J. Chem. Phys.* **1993**, *98*, 5648–5652.
(36) Becke, A. *Phys. Rev. A* **1988**, *38*, 3098–3100.
(37) Yanai, T.; Tew, D.; Handy, N. C. *Chem. Phys. Lett.* **2004**, *393*, 51–57.
(38) Schipper, P. R. T.; Gritsenko, O. V.; van Gisbergen, S. J. A.; Baerends, E. J. *J. Chem. Phys.* **2000**, *112*, 1344–1352.
(39) Ferrighi, L.; Frediani, L.; Fossgaard, E.; Ruud, K. *J. Chem. Phys.* **2006**, *125*, 154112.
(40) Tozer, D. J.; Peach, M. J. G.; Le Sueur, C. R.; Ruud, K.; Guillaume, M. *Phys. Chem. Chem. Phys.* **2009**, *11*, 4465–4470.
(41) Peach, M. J. G.; Benfield, P.; Helgaker, T.; Tozer, D. J. *J. Chem. Phys.* **2008**, *128*, 044118.
(42) Silvers, S. J.; Tulinsky, A. *J. Am. Chem. Soc.* **1967**, *89*, 3331–3337.
(43) Gouterman, M. *J. Mol. Spectrosc.* **1961**, *6*, 138–163.
(44) Schaffer, A. M.; Gouterman, M. *Theor. Chem. Acc.* **1972**, *25*, 62–68.
(45) Nguyen, K. A.; Pachter, R. *J. Chem. Phys.* **2001**, *114*, 10757–10767.
(46) Gouterman, M.; Snyder, L. C.; Wagniere, G. H. *J. Mol. Spectrosc.* **1963**, *11*, 108–128.